J Solid State Electrochem (1998) 2: 221–236

ORIGINAL PAPER

Boris Orel · Marjeta Maček · Jože Grdadolnik
Anton Meden

In situ UV-Vis and ex situ IR spectroelectrochemical investigations of amorphous and crystalline electrochromic Nb_2O_5 films in charged/discharged states

Received: 21 August 1997 / Accepted: 9 October 1997

Abstract Niobium oxide (Nb_2O_5) films and powders have been obtained via the sol-gel route from an $NbCl_5$ precursor. XRD spectra revealed that films with pseudohexagonal (TT-phase) and orthorhombic (T-phase) structure were formed at 500 °C and 800 °C, respectively, while at 300 °C films were amorphous. Infrared (IR) and Raman spectra of powders and films of Nb_2O_5 in different polymorphic forms were detected, and vibrational band assignments were made. Electrochromic properties of amorphous films and films with the TT-phase were established from in situ ultraviolet visible (UV-Vis) spectroelectrochemical measurements and correlated with ex situ IR transmission spectra of charged films. Ex situ IR spectra revealed that charging of amorphous films is accompanied by variations of the Nb-O stretching mode intensity, while, for films with the TT- and T-phase, splitting of the Nb_3-O stretching modes and the appearance of polaron absorption were noted with Li^+ ion insertion. Ex situ X-ray diffraction (XRD) spectra of charged films with the TT-phase showed changes of the unit cell dimensions with charging. The influence of the polaron absorption on the ex situ near-grazing incidence angle (NGIA) IR reflection-absorption spectra of charged/discharged films is discussed in detail.

Key words Niobium oxide · Infrared spectroscopy
Films · Electrochromism

B. Orel (✉) · M. Maček · J. Grdadolnik
National Institute of Chemistry, Hajdrihova 19,
1001 Ljubljana, Slovenia
Tel.: +386-61-1760-276; Fax: +386-61-1259-244;
e-mail: Boris.Orel@ki.si

A. Meden
Faculty of Chemistry and Chemical Technology,
University of Ljubljana, Aškerčeva 5, 1001 Ljubljana, Slovenia

Introduction

Niobium oxide (Nb_2O_5) is a promising electrochromic (EC) material for "smart" window applications [1]. Nb_2O_5 is known to have various polymorphic forms [2, 3] among which the H-phase [3] obtained at temperatures above 1000 °C is the most thermodynamically stable. The H-phase exhibits a complex structure [4] originating from the existence of superstructures comprising 3×5 and 3×4 ReO_3 type blocks [5] of NbO_6 octahedra sharing corners and edges. Alternatively, T- [6] and TT- [7, 8, 9] phases, which are stable at 650–800 °C and 300–550 °C, respectively, do not consist of ReO_3 blocks and are characterized by three-dimensionally linked structures formed from corner- and edge-sharing octahedra and pentagonal bipyramids.

Nb_2O_5 exhibits a wide variety of properties depending on its crystalline modification. The H-phase exhibits a high dielectric constant (~100) [10], whereas the T-phase attracted interest because of its remarkably high electrochemical stability and excellent cycling behavior [11]. Accordingly, it was tested as a negative electrode in rechargeable rocking-chair batteries [12] using V_2O_5 as an anode.

The TT-phase is of particular interest for electrochromism [1]. Recently, Avellaneda et al. [13–15] showed that Nb_2O_5 with the TT-phase could be ranked among the best cathodic electrochromic films, exhibiting similar electrochromic effects to the more extensively investigated WO_3 [16]. Insertion of Li^+ ions changed the transmittance of the films from 78% to 24% ($\lambda = 600$ nm), and coloring/bleaching kinetics was up to 10 s [13]. The Nb_2O_5 films exhibit a high transparency in the bleached state, and their color in the charged state is neutral, contrasting with the deep blue cathodic coloration of WO_3. Recently, we have improved the bleaching kinetics of Nb_2O_5 films with the TT-phase by making lithiated ($Li_{0.4}NbO_{5.2}$ and $Li_{0.2}Nb_2O_{5.1}$) films using the sol-gel route and $NbCl_5$ precursors [17, 18].

Amorphous films obtained by heat treatment at 300 °C [17, 18] are also electrochromic, but they exhibit smaller coloring/bleaching changes in the near-IR spectral range ($T_{colored}$-$T_{bleached} \approx 35\%$ at $\lambda = 634$ nm), and the transparency of the films in the bleached state is less (~75%) than that of films with the TT-phase [13, 17, 18]. For these reasons, and because their ion-storage capacity is 20 mC/cm^2, they have been proposed as a counter-electrode for EC devices with anodic NiO_x films [19, 20]. Hydrated amorphous niobium oxide films ($Nb_2O_5 . nH_2O$) [9, 17, 18], consisting of distorted pentahedra, hexahedra and octahedra as structural units, are not electrochromic but have found a use in catalytic applications [21].

Nb_2O_5 films have been prepared by thermal oxidation of the metal [22, 23], anodic deposition [24, 25], sputtering, [12, 26, 27], vacuum evaporation [28] and via the sol-gel route [13–15, 17, 18, 29–31]. For large-area EC device applications, however, sputtering and vacuum evaporation depositions have certain advantages over sol-gel and dip-coating deposition.

The structural changes which are caused by Li^+ insertion were studied by XRD [11] and X-ray photoelectron spectroscopy (ESCA) [11, 19, 20]. Shifts of the O1s, Li1s Nb3d$_{3/2}$ and Nb3d$_{5/2}$ peaks of powders possessing the T-phase [11] revealed strong $Li^+ \ldots O^{2-}$ interactions and confirmed the formation of the Nb^{4+} species in Li^+-inserted films. Smaller shifts were found for amorphous films prepared at 300 °C [19, 20]. The XRD spectra of powders with the T-phase [11] showed redistribution of the atomic arrangement in Li^+ ion-inserted films which, contrary to expectations, did not lead to any change in the unit cell dimensions. This agrees the excellent cycling behavior of the T-phase of Nb_2O_5 [11].

IR and Raman spectroscopy have long been recognized as powerful techniques for the detection of structural changes accompanying Li^+ ion insertion/extraction processes [32]. In our laboratory we have performed extensive IR spectroscopic investigations of various anodic (Ni hydroxide [33], Ni(Si) oxide [34], Co_3O_4 [35], Co(Al, Si) oxide [36], γ-Fe_2O_3 [37]) and cathodic (PWA, TiO_2) [38, 39]) films. Recently, we have reported ex situ IR spectra of sol-gel-derived Nb_2O_5 films performed on dip-coated films deposited on SnO_2:F-coated electrodes [17, 18]. Results of near-normal (6 °) reflection/absorption spectra of charged films enabled us to establish Li^+-O^{2-}-Nb^{4+} interactions, and films having the TT-phase also showed the possible appearance of polaron absorption [17]. NGIA IR ex situ spectra of films in charged/dicharged states, although corroborating the presence of a strong polaron mode in spectra of charged films, also revealed the unusual and still poorly explained effect that charging of films is accompanied by decrease of the intensity of the reflection/absorption bands observed in NGIA IR spectra.

Extensive Raman spectra investigations of various Nb_2O_5 phases [40] and niobium oxide reference compounds exhibiting slightly ($KNbO_3$, $NaNbO_3$ and $LiNbO_3$) and strongly [($K_8Nb_6O_{19}$, $AlNbO_4$ and $Nb(HC_2O_4)_5$] distorted corner- and edge-sharing NbO_6 octahedral structural units have been reported by Jehng et al. [41]. The influence of mechanical and thermal treatment on the IR spectra of H-Nb_2O_5 have been studied by Ikeya et al. [9], and vibrational bands characterizing TT- and T-phases of treated and untreated powders have also been established. However, no IR transmission spectra of Nb_2O_5 films in different polymorphic forms (i.e., TT-, T- and amorphous phases) have been reported so far.

Thus, the main objective of this paper was to obtain IR transmission spectra of xerogel, amorphous and crystalline films with the TT- and T-phases deposited on Si wafers. Also, for films exhibiting the electrochromic effect, we aim to correlate their structure with the IR spectra of films in the colored and bleached states. We focused attention on transmission spectra of films because the transverse optical (TO) vibrational mode frequencies, corresponding to maxima of the imaginary part of dielectric function ($\tilde{\varepsilon}$) (i.e. $\mathrm{Im}(\tilde{\varepsilon}) = 2nk$ [42]) are free of the interfering polarization effects, which are typical of spectra of powders [37, 43]. In addition, near-normal (6 °) reflection spectra of pressed powders were also measured with the aim of gaining knowledge about refractive index (n) and absorption coefficient (k) obtained from a Kramers-Krönig analysis. From the results of Kramers-Krönig analysis frequencies of longitudinal optical (LO) modes corresponding to the maxima of $\mathrm{Im}(-1/\tilde{\varepsilon})\{\mathrm{Im}(-1/\tilde{\varepsilon}) = 2nk/[(n^2 - k^2)^2 + 4n^2k^2]\}$ and TO modes were obtained [42]. This enabled us to establish LO-TO mode splitting and compare the calculated LO frequencies with experimentally obtained values using NGIA IR spectroscopy. LO-TO splitting gave information about the ionicity of Nb_2O_5 crystalline and amorphous films, allowing us to correlate the present polaron mode with the observed coloring/bleaching changes detected from in situ UV-Vis measurements. Simple model calculations of LO spectra were also performed in order to envisage the behavior of the LO modes during charging/discharging of films.

Experimental

The films and powders of studied compounds were prepared as reported in references [17, 18].

The Fourier transform infrared (FT-IR) and FT-Raman (excitation wavelength 1064 nm) spectroscopic measurements were performed using a Perkin-Elmer System 2000 Spectrometer (at resolutions 4 cm^{-1} and 8 cm^{-1}). Transverse optical (TO) modes were obtained from IR transmission spectra of films deposited on infrared transmitting Si wafers (electrical resistivity 200 Ω cm). For detection of longitudinal optical (LO) modes of the films, the spectroscopic cell with near-grazing incidence angle (NGIA) (80 °) geometry and p-polarized light were used. In this case, films were deposited on IR-reflecting fluorine-doped tin-oxide-coated glass substrates (SnO_2:F, K-glass, Pilkington). Reflection spectra of powders pressed into pellets were measured at near-normal inci-

dence angle (6 °), and the refractive index (n) and absorption coefficient (k) were calculated using the Kramers-Krönig analysis available on the PE2000 System. Thickness measurements were done on a Surface Profiler Alfa Step 200 with resolution 5 nm. XRD measurements were made using a Philips PW 1710 automated X-ray diffractometer.

Cyclic voltammetric (CV) and chronocoulometric (CPC) experiments were performed using an EG & G PAR model 273 computer-controlled potentiostat-galvanostat, driven by the 270 Electrochemical Analysis software. A three-electrode system was employed. The working (test) electrode consisted of a 3-cm^2 glass slide covered with an SnO_2:F coating onto which niobium oxide was deposited. The slide was in physical contact with an electrolyte solution of 1 M $LiClO_4$ in propylene carbonate (PC). A Pt rod served as a counter electrode and Ag/AgCl/1 M LiCl in methanol as the reference electrode. During cyclic voltammetry, a potential scan rate of 10 mV/s was used.

In situ UV-Vis spectroelectrochemical measurements were performed on an HP845X UV-Vis system diode array spectrophotometer with an EG & G PAR model 273 computer-controlled potentiostat-galvanostat. The spectra were recorded, taking as a background the spectrum of a spectroelectrochemical cell filled with the electrolyte (1 M $LiClO_4$/PC). The coloring/bleaching changes of the films were measured relative to this background.

Results

XRD spectra of powders and films with the TT- and T-phase

Powders obtained after heating xerogels at 300 °C, 500 °C and 800 °C for 15 min were examined using XRD analysis. A comparison between the XRD spectra (Fig. 1) and the PDF files [44] revealed that the powders heated at 500 °C correspond to the TT-Nb_2O_5 phase, possessing a pseudohexagonal structure (PDF 28-317 and PDF 7-61), while those heat treated at 800 °C correspond to the T-Nb_2O_5 phase, with an orthorhombic structure (PDF 27-1003). Other than the slight shifts in 2Θ values of peaks, these phases could be easily differentiated, the closely spaced peaks at 28.30 °, 28.86 ° and 36.52 °, 36.98 ° being characteristic of the T-phase, while single peaks ($2\Theta = 28.46$ ° and $2\Theta = 36.66$ °) were formed in XRD spectra of the TT-phase. Accordingly, at intermediate temperatures (~650 °C) both phases appeared simultaneously. However, at extended heating times (~2 h) at temperatures below 300 °C, the TT-phase was not formed. This is an advantage of the sol-gel route, which yields pure TT- and T-phases in a relatively narrow temperature interval and with short heat-treating times (15 min). This contrasts with the preparation of Nb_2O_5 layers by oxidizing metal at 500 °C, bringing about the T-phase [11] or one of the existing Nb_2O_5 phases [22]. In order to exclude the possible formation of mixed phases during dip-coating deposition, XRD spectra of films were obtained. Up to nine successive dippings were needed to make sufficiently thick films to obtain satisfactory XRD peaks (Fig. 2). Films which were deposited either on glass or SnO_2:F-coated glass brought about almost identical XRD spectra, the difference being the additional peaks at $2\Theta = 37.9$ ° and $2\Theta = 51.7$ ° belonging to SnO_2:F.

Spectroelectrochemical measurements of amorphous films and films with the TT-phase

CV responses of films were measured at a scan speed 10 mV/s in the potential range +2.0 to −1.7 V vs Ag/AgCl in order to avoid Li^+ ion insertion into the underlying SnO_2:F layers [45, 46]. The CV response of amorphous as-deposited film differs considerably from that of cycled films (Fig. 3). A less pronounced difference was noted between the CV responses of crystalline films with the TT-phase (Fig. 4). Both kinds of films required only a few cycles to attain a reversible current response. A stable CV response is achieved for crystalline films after three cycles, while six cycles are necessary to stabilize amorphous films.

Monochromatic transmittance measurements ($\lambda = 634$ nm) with the accompanying CV responses are depicted in Figs. 5 and 6. The results revealed that the transmittance of amorphous films in the bleached state decreases from 90% in as-deposited film to 75% in film after cycling six times, while the transmittance of films in the colored states did not change during the stabilization period and remained at about 40%. Conversely, the monochromatic transmittance of the crystalline films in the colored and bleached states showed little change, with cycling remaining at 20% and 90%, respectively. It should be noted that the highest coloring of crystalline films is attained at the highest cathodic potentials. This contrasts with the coloring of amorphous films, where the highest coloring is reached at less negative potentials, coinciding with zero current density values (Figs. 5 and 6).

The coloring/bleaching kinetics of the films was established from chronocoulometric (CPC) measurements performed by charging/discharging of films at limiting potentials (+2.0 V and −1.7 V) for 120 s. While the coloring of both kinds of film takes place at the same speed, amorphous films did not achieve their full bleaching after 120 s, unlike the crystalline films, which became fully bleached after being discharged for 120 s (Fig. 7).

The spectra of amorphous and crystalline films in as-deposited, bleached and colored states are shown in Fig. 8. The most important feature of the spectra of colored crystalline films is the low transmittance extending into the spectral range, while the near-IR transmittance of the colored amorphous films increases to higher values with increasing wavelengths. In this respect, the crystalline films behave similarly to amorphous WO_3 films, exhibiting polaron absorption in the Li^+-ion-inserted state [1, 17, 18] (see below). The coloration efficiency (CE) (defined as the change of the optical densities of films in colored and bleached states divided by the inserted charge) of the crystalline films is in the order of 25–31 cm^2/C, outranging that of the amorphous films, which is no higher than 18 cm^2/C [17]. Spectroelectrochemical measurements of films possessing the T-phase have not been done because the heat-treatment temperature of this type of film is too high

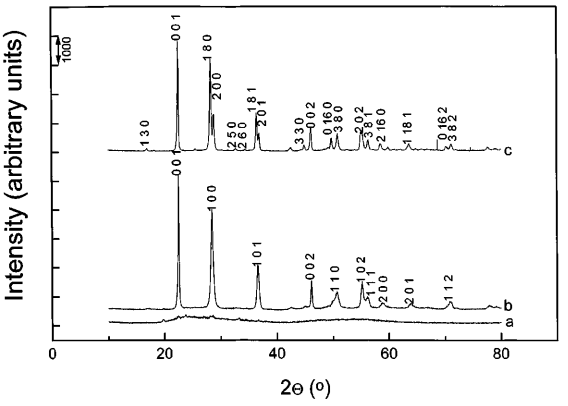

1

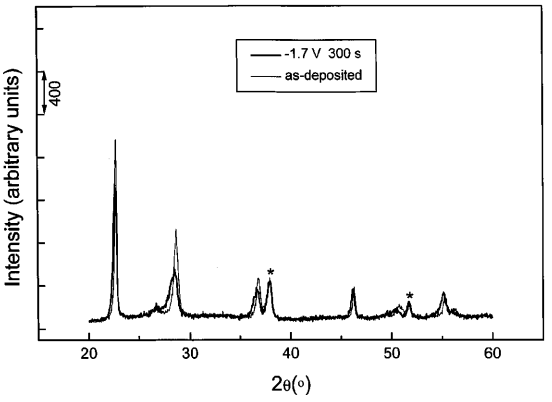

2

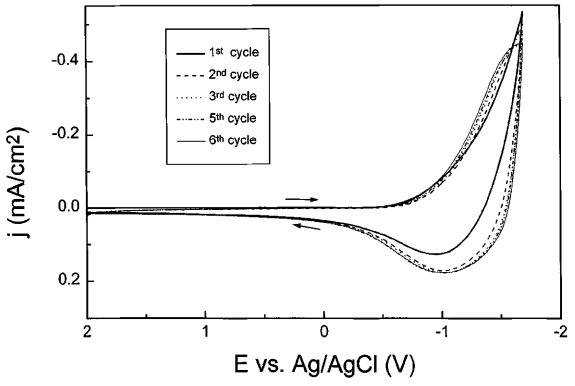

3

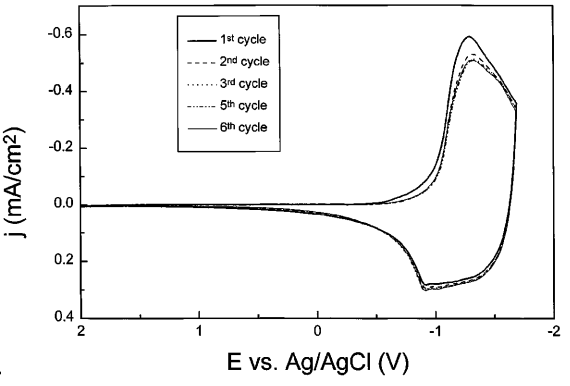

4

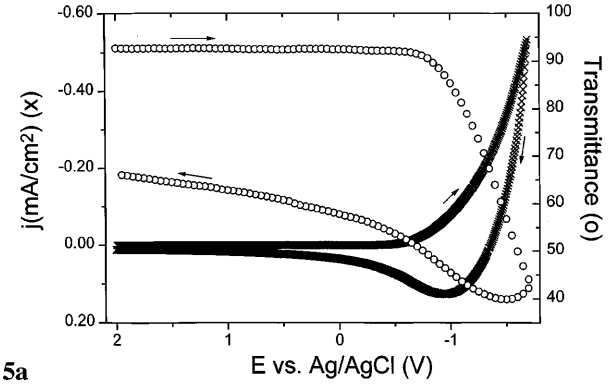

5a

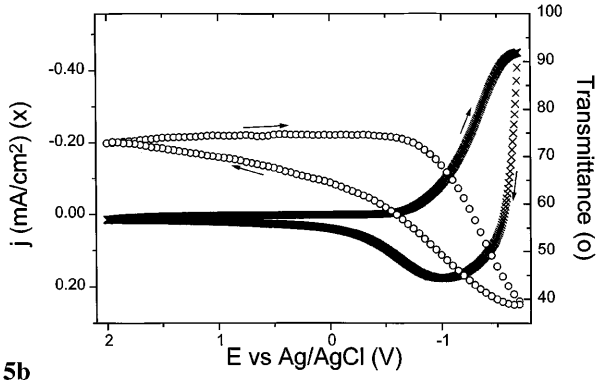

5b

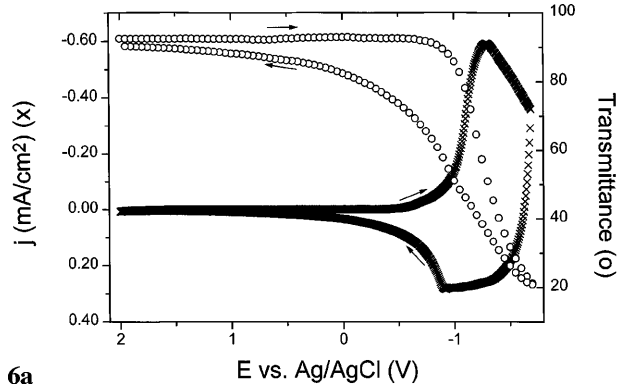

6a

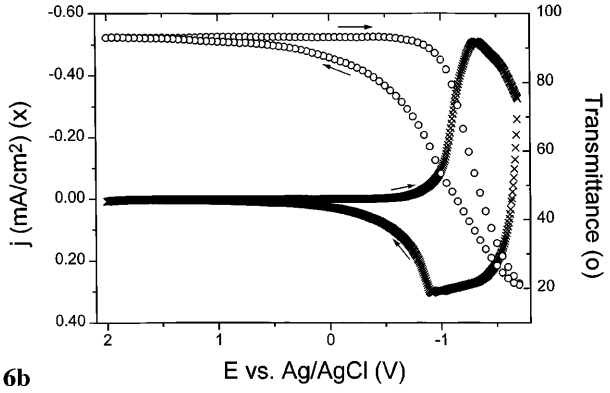

6b

◄

Fig. 1a–c XRD spectra of Nb_2O_5 powders: **a** amorphous (300 °C), **b** TT-phase (500 °C) and **c** T-phase (800°C)

Fig. 2 XRD spectra of as-deposited Nb_2O_5 film [obtained with nine successive dippings (thickness ~ 900 nm)] and after charging at –1.7 V for 300 s. * → Asterisks (*) indicate peaks belonging to SnO_2:F

Fig. 3 CV responses of amorphous Nb_2O_5 film (prepared by heat treatment at 300 °C for 15 min) cycled in the potential range from 2.0 V to –1.7 V vs Ag/AgCl in 1 M $LiClO_4$/PC electrolyte, scan speed 10 mV/s

Fig. 4 CV responses of Nb_2O_5 film with TT-phase (prepared by heat treatment at 500 °C for 15 min) cycled in the potential range +2.0 V to –1.7 V in 1 M $LiClO_4$/PC electrolyte, scan speed 10 mV/s

Fig. 5a, b CV responses (x) and monochromatic transmittance (λ = 634 nm) measurements (o) of amorphous Nb_2O_5 film (thickness = 140 nm) in 1 M $LiClO_4$/PC electrolyte in the potential range +2.0 V to –1.7 V vs Ag/AgCl reference electrode. Scan speed 10 mV/s; **a** 1st cycle, **b** 6th (stabilized) cycle

Fig. 6a, b CV responses (x) and monochromatic transmittance (λ = 634 nm) measurements (o) of crystalline Nb_2O_5 film with TT-phase (thickness = 132 nm) in 1 M $LiClO_4$/PC in the potential range +2.0 V to –1.7 V vs Ag/AgCl reference electrode. Scan speed 10 mV/s; **a** 1st cycle, **b** 6th (stabilized) cycle

(~800 °C), preventing their deposition on SnO_2:F-coated glass.

Vibrational spectra

Before considering vibrational spectra of samples, a few remarks about the structural features of Nb_2O_5 should be made. A unit cell of the pseudohexagonal structure of the TT-phase can best be described as the structure of α-UO_3 [4] taking into account that O(II) below or above the *ab* crystal plane represents oxygen vacancies (Fig. 9a, b). Each Nb atom is surrounded by 6, 7 or by 8 oxygen atoms, making a construction unit of a tetra-, penta- or hexagonal bipyramid linked along the *c* crystal axis by collinear Nb-O-Nb bridging bonds [9, 41].

In contrast to the TT-phase, the orthorhombic T-phase obtained by heat treatment at 800 °C does not possess oxygen vacancies (Fig. 9c). As a result, each Nb atom is surrounded by six or seven oxygens, forming distorted octahedra or bipyramids. These polyhedra are joined by edge or corner sharing in the *ab* plane and by corner sharing along the *c* axis. The structure of the T-phase is therefore more compact than the TT-phase [9, 41]. The structure of the xerogel is considered to consist of slightly distorted NbO_6, NbO_7 and NbO_8 polyhedra [26, 41], with water molecules bonded to the oxygens by OH...O bonds of various strengths.

Structural features of niobium oxide phases imply specific vibrational modes which are characteristic of the particular structures. The vibrational band assignment of the Nb_2O_5 phases is based on IR spectra of similar compounds such as Gatehouse tungsten bronzes [47], columbite [48] and mechanically and thermally treated Nb_2O_5 powders [9].

Three relatively ill-defined groups of vibrational modes assigned to Nb = O terminal, Nb-O-Nb bridging and Nb_3-O stretching modes appearing in the spectral ranges 910–850 cm^{-1}, 850–580 cm^{-1} and 500–380 cm^{-1}, respectively, characterize the spectra of niobium oxide in different phases. Specifically, for T- and TT-phase, where no Nb = O terminal groups except those belonging to the surface groups were predicted, three different types of Nb-O stretchings were observed: the collinear Nb-O-Nb stretch (850–800 cm^{-1}), the Nb_3O stretching at relatively low frequencies (500–400 cm^{-1}) and the bridging Nb-O-Nb stretch appearing at frequencies intermediate between the two former modes (750–580 cm^{-1}). Bands belonging to each of the specific modes are expected to show multiple bands depending on the symmetry of the particular phase and the type of interactions, originating from the way in which polyhedra are linked together.

The vibrating dipoles of the bridging Nb-O-Nb lie in the T- and TT-phase in the *ab* crystal plane and are related to Nb-O-Nb bridging modes of the edge-sharing polyhedra. The collinear Nb-O-Nb stretching vibrates in T- and TT-phases along the *c* crystal axis (Fig. 9). The Nb_3-O stretch is solely characteristic of the pseudohexagonal TT- and orthorhombic T-phase, while it is not expected to appear in spectra of xerogels consisting of small clusters of variously linked polyhedra. However, the collinear Nb-O-Nb stretchings may be admitted for clustered niobium polyhedra, which are present in xerogels. Nb = O terminal bond modes predicted for xerogels can appear also in higher temperature phases, where surface Nb = O groups may be present.

Sols, gels and xerogels

When sol is dropped onto a CdTe plate it quickly dries. The initial spectrum (Fig. 10) still shows plenty of bands originating from the propanol; however, the bands at 597 cm^{-1} [ν_3(Nb-O)], 913 cm^{-1} [ν(Nb = O)], 844 cm^{-1} [collinear ν(Nb-O-Nb)] and the weak shoulder band at 784 cm^{-1} could be seen in the spectra obtained after 10 min. After 110 min the intensity of the 597 cm^{-1} band increases considerably and shifts to 567 cm^{-1}, while the 913 cm^{-1} band exhibiting the highest intensity in the spectrum of fresh sol decreased in intensity (Fig. 10). This indicates that in a fresh sol at least partially condensed polyhedra exist linked across their corners (844 cm^{-1}, 784 cm^{-1} bands). The terminal Nb = O bands (913 cm^{-1}), however, prevail in the sol. With drying, condensation of polyhedra proceeds, which could be judged from the decrease of the 913 cm^{-1} band (Nb = O terminal stretch) and the increase of the 567 cm^{-1} band (asymmetric Nb-O streching mode [ν_3]) [49]. IR spectra of xerogels obtained after 110 min (Fig. 10) do not contain any traces of propanol; however, OH...O stretching (~3300 cm^{-1}) and bending modes (1640 cm^{-1}) signaling the hydrogen-bonded water became quite intense.

Raman spectra of xerogel powders (Fig. 11, spectrum a) exhibit Nb = O terminal stretch at 911 cm^{-1}, the Nb-O stretch originating from the totally symmetric mode

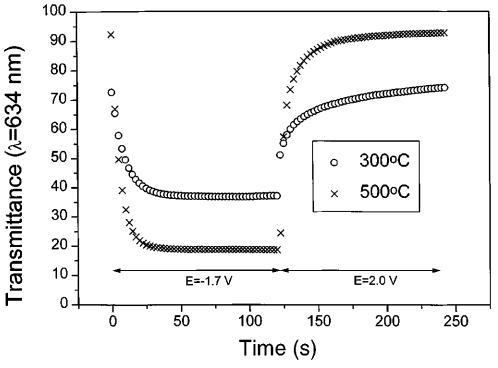

7

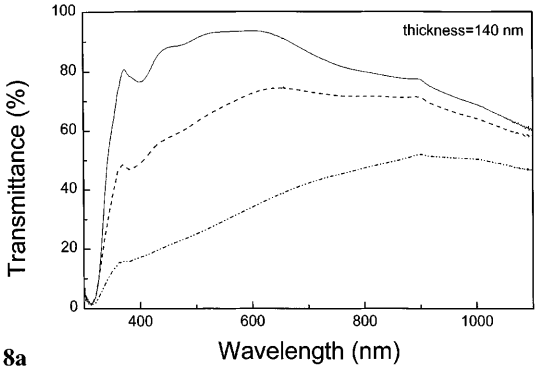

8a

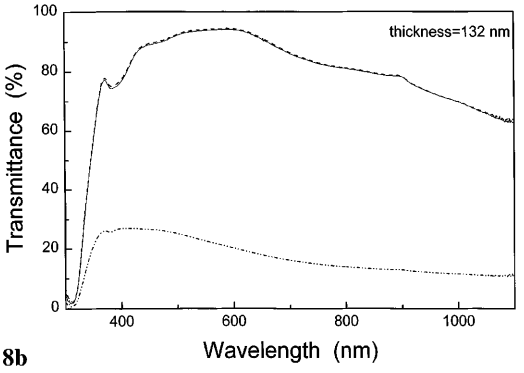

8b

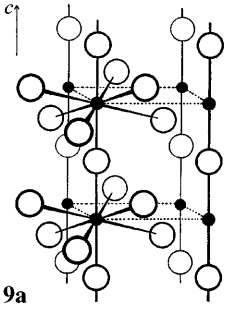

9a

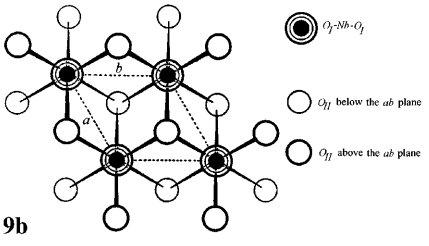

9b

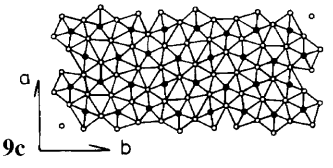

9c

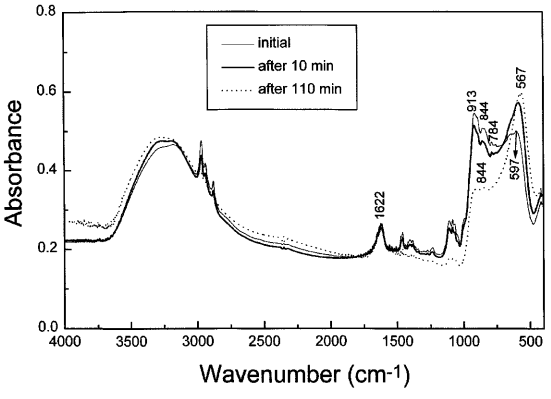

10

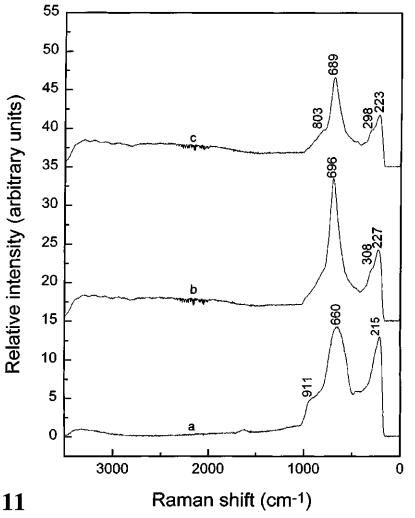

11

◀

Fig. 7 Monochromatic transmittance ($\lambda = 634$ nm) changes during coloring (at –1.7 V) and bleaching (at 2.0 V) of amorphous (300 °C) and crystalline (500 °C) Nb_2O_5 films

Fig. 8a, b In situ UV-Vis spectral transmittance measurements of Nb_2O_5 films heat treated at **a** 300 °C and **b** 500 °C obtained by charging at the limiting potentials –1.7 V (-···-) and + 2.0 V (- - -); as-deposited (——)

Fig. 9a–c Crystal structure of **a** the pseudohexagonal TT-phase **b** viewed perpendicular to the *c* axis and **c** T-phase of Nb_2O_5 [9]. In the TT-phase (**a**, **b**) [4], oxygens O(II) below or **O**(II) above the *ab* plane represent vacant sites, O(I)-Nb-O(I) group with axis along *c* axis and Nb in the *ab* plane

Fig. 10 IR transmission spectra of drying sol deposited on CdTe plates

Fig. 11a–c Raman spectra of Nb_2O_5 powders: **a** xerogel, **b** TT-phase and **c** T-phase

(v_1) of niobium oxide polyhedra at 660 cm^{-1} [49] and the Nb-O-Nb deformational mode at 215 cm^{-1}. All modes conform well to those already reported for Raman spectra of amorphous $Nb_2O_5 \cdot nH_2O$ [41]. The Raman spectra of powders with TT- and T-phase are also in agreement with published data [9, 41] (Table 1 and Fig. 11, spectra b and c).

Powders and films

IR spectra of xerogel powder and powders obtained at 300 °C, 500 °C (TT-phase) and 800 °C (T-phase) are shown in Fig. 12. The results revealed that IR spectra of powders are pronouncely broader and that the relative intensities of bands differ considerably from those observed in the spectra of the films (Fig. 13). For example, a single band corresponding to the Nb-O stretching, which appears at 670 cm^{-1} in the spectra of amorphous powders prepared by heat treatment at 300 °C, revealed in the spectra of films three well-resolved bands at 635 cm^{-1}, 582 cm^{-1} and 516 cm^{-1} (Fig. 13 and Table 1). Even more pronounced differences between the spectra of films and powders were noted for the TT-phase. While in the spectra of the films the most intense band appears at 500 cm^{-1}, three bands with the strongest at 614 cm^{-1} and two shoulder bands at 670 cm^{-1} and 600 cm^{-1} (marked with an asterisk) appeared in the spectra of the corresponding powders. Also the intensity of the collinear Nb-O-Nb stretching mode appearing in powder spectra at 812 cm^{-1} is considerably stronger than in the spectra of films. An additional shoulder band at 858 cm^{-1}(Fig. 12) could also be seen in spectra of powders.

The differences observed in the spectra of the films and powders can be explained by the polarization effect. This is caused by the Coulombic field associated with the strong polar modes which exist in Nb_2O_5 [43]. Thus, because of the Coulombic field interactions between the niobium oxide particles, which have different shapes and sizes, the frequencies observed in IR spectra of powders are shifted from the frequency of the TO modes appearing in spectra of films. This questions the accuracy

Table 1 Assignment and vibrational band frequencies (in cm^{-1}) obtained from the corresponding IR transmission (TO) spectra of films and powders. Raman spectra are given for powders

Assignment	Band frequency											
	Raman spectra of powders			IR transmission spectra of films (TO modes)				IR transmission spectra of powders (in RbI)				
	Xerogel	TT-Nb_2O_5 (500 °C)	T-Nb_2O_5 (800 °C)	Sol	Xerogel	300 °C	TT-Nb_2O_5 (500 °C)	T-Nb_2O_5 (800 °C)	Xerogel	300°C	TT-Nb_2O_5 (500°C)	T-Nb_2O_5 (800°C)
ν(OHO)	3321 w			3276 m	3300 s				3270 s			
				3169 s	3220 m							
δ(OHO)	1627 w			1622 m	1630 m				1616 m			
ν(Nb=O)	911 m sho			913 vs	926 m				930w sho			
Collinear				844 m	847 m	840 m sho		840 w sho	833 m	881 m sho	858 w sho	840 w sho
ν(Nb-O-Nb)			803 w sho				800 m sho	800 m			812 s	815 s
				784 m				712 w sho			710 w sho	725 w sho
v_1(Nb-O)	660 vs	696 vs	689 vs							670 vs		
											654 w sho	
Bridging					634 w sho	634 w sho	635 m sho	634 w sho			614 vs	618 vs
ν(Nb-O-Nb)												
v_3(Nb-O)				597 vs	565 vs	582 vs			575 vs	520 w sho		
											575 w sho	580 w sho
ν(Nb_3O)						516 w sho	500 vs	515 w sho				
								465 s				
v_4(Nb-O-Nb)		308 w sho	298 w sho									
	215 vs	227 m	223 m									

of the vibrational mode frequencies of niobium oxide reported so far [9, 41, 47, 48].

In order to get additional evidence that spectra of films more accurately represent the vibrational spectra of various phases, near-normal (6 °) reflection spectra of cold-pressed xerogel, TT- and T-phase powders were measured (Fig. 14), and absorption spectra were calculated from the refractive index (n) and absorption coefficient (k) obtained by the Kramers-Krönig analysis. Results revealed excellent agreement between IR spectra of films and the calculated TO spectra corresponding to the maxima of the imaginary part of the dielectric function ($2nk$) (Figs. 13, 15 and Table 2). For the majority of investigated samples, the agreement is within ± 5 cm^{-1}, which is quite surprising because the reflection spectra of pressed powders are a relatively crude approximation compared to the spectra of monocrystals, such spectra usually being required for Kramers-Krönig analysis. Larger deviation was found between transmission spectra of films and $2nk$ spectra of pressed powders heat treated at 300 °C. This is most likely caused by the variation in the content of partially formed TT-phase in the powders.

Inspection of the band frequencies of xerogel, TT- and T-phases listed in Table 1 shows that the Nb-O asymmetric stretching mode appearing between 600 and 450 cm^{-1} (ν_3 mode according to [49]) shifts to lower frequencies when the structure changes to the more condensed T- and TT-phases. The appearance of the new band at 500 cm^{-1} was assigned to Nb_3O stretching and is characteristic of the TT crystalline phase. In the T-phase, this mode became split (i.e. 515 cm^{-1} and 465 cm^{-1}), indicating lowering of the symmetry of the unit cell from pseudohexagonal (TT-Nb_2O_5) to orthorhombic (T-Nb_2O_5). Splitting of the collinear Nb-O-Nb stretching mode in the spectra of the T-phase to 840, 800 and 712 cm^{-1} further corroborates the decrease of the symmetry.

Fig. 12 IR transmission spectra of **a** xerogel powders and powders prepared by heat treatment at **b** 300 °C, **c** 500 °C and **d** 800 °C. Powders were prepared in RbI pellets

Fig. 13 IR transmission spectra of **a** xerogel films and films obtained by heat treatment at **b** 300 °C (amorphous Nb_2O_5), **c** 500 °C (TT-phase) and **d** 800 °C (T-phase) deposited on Si-wafers

Fig. 14a, b Near-normal (6 °) reflection spectra **a** of cold-pressed powders of xerogel and powders obtained by heat treatment at 300 °C (amorphous Nb_2O_5), 500 °C (TT-phase) and 800 °C (T-phase) and **b** refractive index (n) of samples obtained from Kramers-Krönig analysis

Fig. 15a, b Calculated $2nk$ spectra of **a** xerogels and amorphous Nb_2O_5 powders (300 °C) and **b** crystalline Nb_2O_5 powders prepared at 500 °C and 800 °C

Ex situ IR spectra

Ex situ IR spectra of charged/discharged films were obtained first in the transmission mode, from films deposited on Si wafers. Because of the high ohmic drops, stemming from the relatively low electronic conductivity of the substrate, the potentials used for charging were high and could not be correlated with those found for films deposited on SnO_2:F-coated glass electrodes. This led us to repeat ex situ IR spectral measurements of

Table 2 Experimentally determined TO modes from transmission spectra and LO modes from NGIA IR spectra of films and corresponding calculated TO modes [Im($\tilde{\varepsilon}$)] and LO modes [Im($-1/\tilde{\varepsilon}$)] obtained from Kramers-Krönig analysis of near-normal (6°) reflection spectra of pressed powders

Assignment	experimentally determined TO modes (calculated [Im($\tilde{\varepsilon}$)] frequencies from near-normal reflection spectra of powders)				LO modes from IR NGIA spectra (calculated LO modes from near-normal reflection spectra of powders[a])		
	Xerogel	300 °C	TT-Nb_2O_5 (500 °C)	T-Nb_2O_5 (800 °C)	Xerogel	300 °C	TT-Nb_2O_5 (500 °C)
ν(Nb = O)	926 (918 w sho)						
	847 (816 m sho)	840 (838 m sho)		840 (840 m sho)			
collinear ν(Nb-O-Nb)			800 (800 m sho)	800 (800 m)			
				712 (712 w sho)	773	835	761 (744 m sho)
ν_3(Nb-O)	565 (574 vs)	582 (577 vs)			964		
		516 (486 m)		515 (515 w sho)		948	
ν(Nb_3-O)			500 (510 vs)				968 (945 vs)
				465 (455 vs)			

[a] LO modes were calculated only for TT-phase

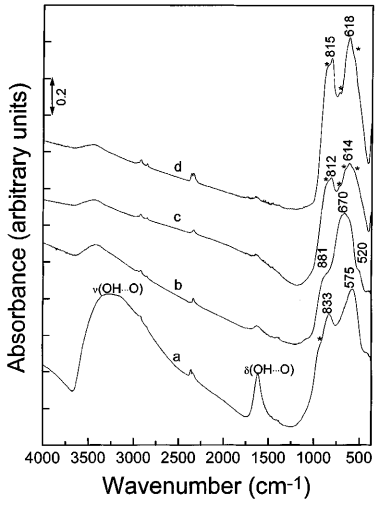

12

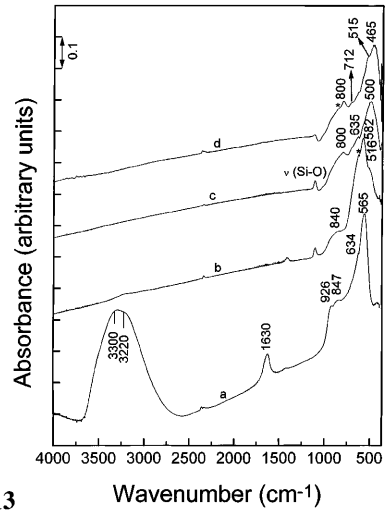

13

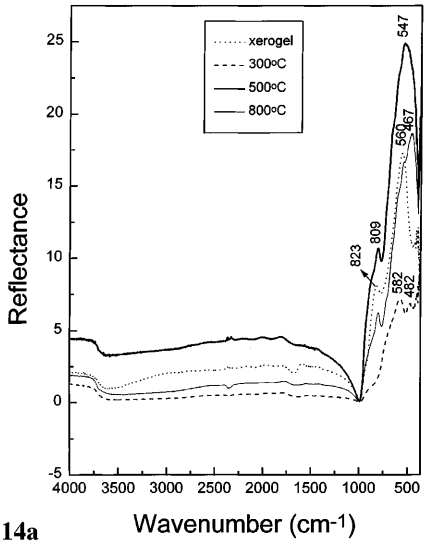

14a

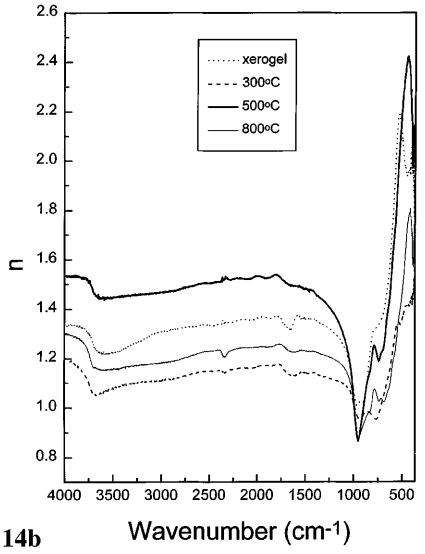

14b

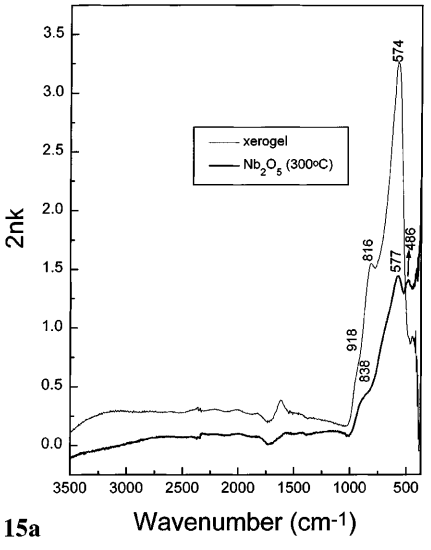

15a

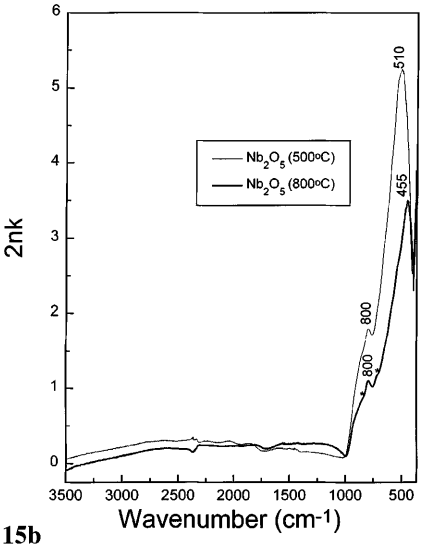

15b

charged/discharged films in the reflection/absorption mode (see below) at NGIA conditions. This is because in these kinds of measurements the films were charged at the same level as in the in situ UV-Vis and corresponding CV measurements.

1. Ex situ IR transmission measurements

Amorphous films (300 °C). Ex situ IR spectra of as-deposited films and films obtained after charging at –10 V (for 480 s) and discharging at 10 V for the same time are represented in Fig. 16. The most prominent feature in the spectra is the decrease in intensity of the 577 cm^{-1} band corresponding to the Nb-O stretching mode, which except for the decrease in intensity does not exhibit any frequency change. This is also true for the Nb-O-Nb bridging mode at 634 cm^{-1}. However, the collinear bridging Nb-O-Nb stretch nearly disappears (Table 3). When the films are discharged the spectra of the as-deposited films are restored, except that the intensity of the strongest band at 577 cm^{-1} does not match the intensity which this band exhibited in the spectrum of the as-deposited film. In addition, the width of this band in the spectra of charged films increases, indicating the formation of different sites with closely spaced vibrational energies, lying in the spectral range where Nb_3-O stretching of the TT and T phase appears (< 500 cm^{-1}).

The observed ex situ IR spectra corroborate the results obtained from the in situ UV-Vis spectroelectrochemical measurements (Fig. 8a). Thus, the transmittance of as-deposited films is higher than that of bleached films. Even after prolonged cycling (a few hundred cycles), the transmittance of the bleached state remains at a low level compared to that of the as-deposited films. This suggests that, after the first reduction/oxidation cycle, reduced Nb^{4+} species are retained in the bleached film, lowering its transmittance. This is supported from the inserted/extracted charges (Q_{ins}/Q_{extr}) measured after the 1st, 2nd and 3rd charging. For example, the first charging/discharging gave rise to a Q_{ins}/Q_{extr} of –40 mC/cm^2 /22 mC/cm^2, the next –33 mC/cm^2 /28 mC/cm^2 and the third –32 mC/cm^2 /30 mC/cm^2. The Q_{ins}/Q_{extr} ratio steadily decreases, reaching approximately 1 for films with stabilized coloring/bleaching changes (> 10 cycles).

The decrease in intensity of the 577 cm^{-1} and 840 cm^{-1} bands indicates that the changes in the dipole moment become less polar in character in the charged films, which might be explained by the strengthening of the $Li^+ \ldots O^{2-}$ interactions in the charged films. The small but distinct broadening of the 577 cm^{-1} band also suggests the presence of disorder in the film structure, forming modes with closely spaced energy levels.

TT-Nb_2O_5 (500 °C). Ex situ spectra of as-deposited, charged and discharged films are shown in Fig. 17. The most striking difference between the spectra of charged amorphous (300 °C) films and the TT-Nb_2O_5 films is the presence of a strong and broad absorption resulting from polaron absorption.

These results agree with our previous ex situ IR reflection/absorption studies [17] performed on films deposited on SnO_2 : F coated glass, with the distinction that the spectra presented in Fig. 17 more clearly show the relative intensity changes of the skeletal and the polaron modes. The clearer picture is due to the absence of the interference patterns observed in the previously reported near-normal reflection/absorption spectra [17], which blurred the shape of the vibrational bands and slightly shifted their position in the spectra. It should be also noted that, when charged films are exposed to air, Li_2CO_3 is formed on the surface of the films, bringing about the vibrational modes of the adsorbed CO_3^{2-} ions (1517 cm^{-1}, 1424 cm^{-1}, 864 cm^{-1}). In addition, the SiO_2 mode at 1086 cm^{-1} also appears in the spectra owing to the oxidation of the Si substrate. These bands have no interfering effects on the other modes relevant to the insertion/extraction processes; moreover, modes of adsorbed CO_3^{2-} ions disappeared when the films are discharged.

When films are charged at –10 V for 480 s, the bands characterizing the as-deposited TT phase (795 cm^{-1},

Table 3 TO mode frequencies obtained from ex situ IR transmission measurements of as-deposited, charged and discharged films with corresponding band assignment (see Table 1)

Assignment	Band frequency					
	Nb_2O_5 (300 °C)		TT-Nb_2O_5 (500 °C)		T-Nb_2O_5 (800 °C)	
	As deposited	Charged at −10 V (480 s)	As-deposited	Charged at −10 V (960 s)	As-deposited	Charged at −10 V (960 s)
Collinear ν(Nb-O-Nb)	840 m sho	–	795 m sho	826 m sho	804 m sho	830 m
Bridging ν(Nb-O-Nb)	634 w sho	634 w sho	634 m sho	634 m sho	630 w sho	634 w sho
ν_3(Nb-O)	577 vs	577 m				
				550 vs		550 m sho
ν(Nb_3O)			511 vs		515 w sho	500 m
				479 vs	458 vs	458 vs

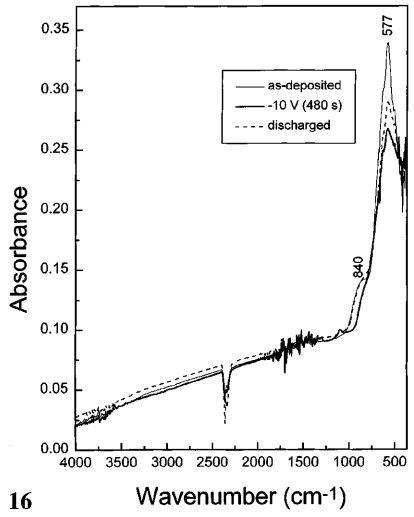

16

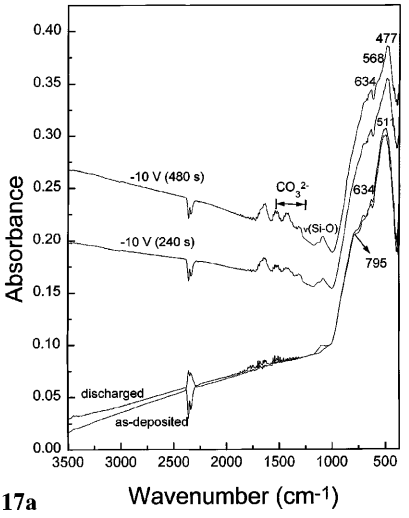

17a

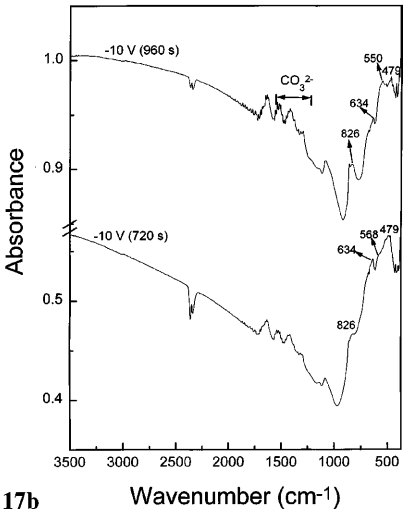

17b

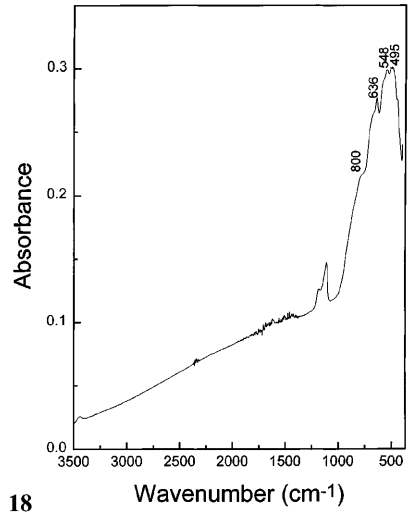

18

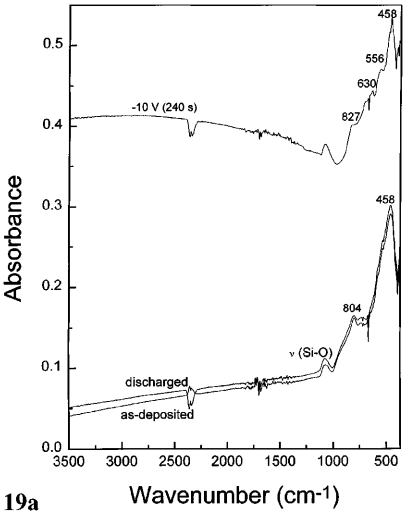

19a

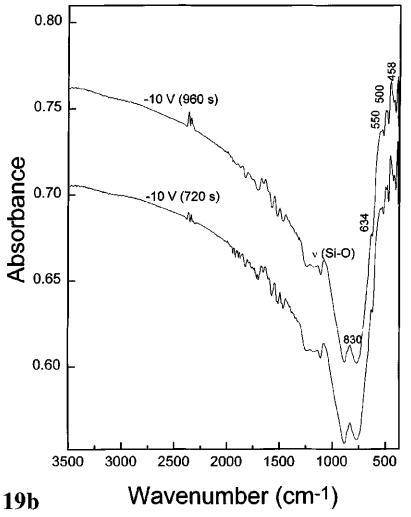

19b

Fig. 16 Ex situ IR transmission spectra of as-deposited amorphous Nb_2O_5 films (obtained by heat treatment at 300 °C for 15 min) deposited on double-sided polished Si-wafer (200 Ω cm). Films were charged at –10 V and discharged at +10 V for 480 s

Fig. 17a, b Ex situ IR transmission spectra of Nb_2O_5 film (TT-phase) prepared by heat treatment at 500 °C. The as-deposited films were charged at –10 V for 240 s, 480 s (**a**) and 720 s, 960 s (**b**). Discharged films were obtained by discharging at 10 V for 960 s (**a**)

Fig. 18 IR transmission spectra (in absorbance units) of lithiated niobium oxide ($Li_{0.4}Nb_2O_{5.2}$) film heat treated at 500 °C

Fig. 19a, b Ex situ IR transmission spectra of Nb_2O_5 film (T-phase) obtained by heat treatment at 800 °C deposited on Si-wafers. As-deposited films were charged at –10 V vs Ag/AgCl in 1 M $LiClO_4$ for 240 s (**a**), 720 s and 960 s (**b**). Discharged films were obtained by discharging at 10 V for 960 s (**a**)

634 cm^{-1}, 511 cm^{-1}) alter in frequency and new bands appear (Table 3), while the collinear Nb-O-Nb stretch shows a blue frequency shift with charging, appearing at 826 cm^{-1} instead at 795 cm^{-1}. The 634 cm^{-1} band is insensitive to charging. In contrast, the 511 cm^{-1} band splits into two at 568 cm^{-1} and 477 cm^{-1}, the 477 cm^{-1} band exhibiting a greater intensity than the 568 cm^{-1} band. Further charging (–10 V, 960 s) leaves the 634 cm^{-1} band unchanged, while the intensity of the split components at 550 cm^{-1} becomes greater than that of the 479 cm^{-1} band. The intensity of the polaron mode also increases, which may be judged from the increasing slope which this band exhibits at wavenumber > 1000 cm^{-1} in the spectra of charged films. Discharging gives rise to spectra identical to those of the as-deposited films. Reversibility is remarkable and is in full agreement with the results of in situ UV-Vis spectroelectrochemical measurements of films and with their electrochemical behavior [13–15, 17, 18]. Lithiation influences to a lesser extent the collinear Nb-O-Nb stretching mode, which exhibits a small albeit distinct blue ($\Delta\nu \sim 30$ cm^{-1}) shift instead of a red shift as was noted for the amorphous (300 °C) films [17]. The existence of interactions between the Nb_3-O stretching mode and the Li^+ ions may be envisaged from the transmission spectra of $Li_{0.4}Nb_2O_{5.2}$ films [17], where the corresponding Nb_3-O stretching is

also split into 548 cm^{-1} and 495 cm^{-1} components (Fig. 18).

The splitting of Nb_3-O stretching modes in charged films is related to the change in the unit cell dimensions, which were determined from the ex situ XRD spectra of the charged film (Fig. 2). All peaks in the XRD spectra of the film charged at –1.7 V for 300 s (Q_{ins} = –241 mC/cm^2) shift to lower 2Θ values and become broader. These changes in the unit cell dimensions were calculated using least square fit of the *d* values that correspond to the pseudohexagonal unit cell to the observed XRD peaks. Results revealed an increase in the unit cell along the *a* axis for about 0.5(1)%, while along the *c* axis the increase is only 0.2(1)%. Changes of the unit cell dimensions, albeit small, indicate anisotropic expansion of the unit cell [$100 \cdot \Delta V/V = 100 \cdot (V_{charged}$-$V_{as\text{-}deposited})/V_{as\text{-}deposited} = 100 \cdot (44.80\ Å^3 - 44.32\ Å^3)/44.32\ Å^3 = 1.1(1)\%$] with Li^+ ion insertion.

T-phase (800 °C). Ex situ IR spectra of as-deposited, colored and bleached films with the T-phase are shown in Fig. 19. As expected, charging gives rise to the polaron mode, which for this phase has not been reported in the IR spectral range. The collinear Nb-O-Nb mode in spectra of charged films (–10 V 240 s), like the TT-phase, exhibits blue shifts (827 cm^{-1}), and a new band at 556 cm^{-1} appears. Further charging (–10 V for 720 s and 960 s) brings about splitting of the Nb_3-O stretching mode, resulting in the appearance of the 500 cm^{-1} band as well as the already noted 550 cm^{-1} and 458 cm^{-1} bands (Table 3). The polaron band is intensified as well. Splitting of the Nb_3-O stretching modes indicates that these modes are affected to the greatest extent when Li^+ ions are inserted in the films, suggesting a decrease of the effective symmetry of Nb-O polyhedra due to the $Li^+ \ldots O^{2-}$ interactions. This is in accordance with the strong $Li^+ \ldots O^{2-}$ interactions determined from the ESCA spectra of charged powders with the T-phase [11]. Disordering is related to the *ab* crystal plane, agreeing with the large dimensions of the *b* axis (i.e. 29.312 Å [44]), while disordering along the shorter *c* axis is not observed. This agrees with the orientations of the changes in the dipole moment of the collinear Nb-O-Nb and Nb_3-O stretching modes.

2. Ex situ NGIA IR spectra of films

Amorphous (300 °C) and TT-Nb_2O_5 (500 °C). LO modes obtained from NGIA IR reflection/absorption measurements of various films prepared at different temperatures differ considerably with respect to TO modes observed in the transmission spectra (Figs. 13, 20). In order to attribute each of the observed LO bands in the NGIA IR spectra to their TO counterparts, the LO modes were calculated from the refractive index (*n*) and absorption coefficient (*k*) obtained from Kramers-Krönig analysis of near-normal reflection spectra of powders pressed into self-supporting thick (~2 mm) pellets. Results revealed that the strongest band in NGIA IR spectra is attributed to the strongest TO band appearing in transmission spectra (Table 2, Figs. 13, 20). The general appearance of the calculated LO spectra (not shown) and measured spectra are in good agreement, confirming the correctness of the applied procedure.

The NGIA IR (LO) spectra of the amorphous films (300 °C) charged at the same level as those treated electrochemically and spectroelectrochemically show a continuous red shift accompanied by a decrease in intensity. This frequency shift that occurs with charging is linear and can be correlated with the steady decrease in the intensity of the TO mode (Figs. 16, 21). Conversely, LO modes of films with the TT-phase completely disappear in the spectra of charged films (Fig. 22) (see below). This contrasts with the presence of the split Nb_3-O stretching in TO spectra of charged films (Fig. 17). Similar extinction of the band intensity, accompanied by the small red shift of the LO mode, were also detected for charged amorphous WO_3 films, which exhibit similar strong polaron absorption extending from the Vis-near-IR spectral range towards the spectral region where the skeletal modes appear [17]. Conversely, other electrochromics such as Ni hydroxide and Co_3O_4 do not show such behavior of LO modes in the charged NGIA IR spectra, in accordance with the fact that no polaron absorption was detected in the vicinity of the skeletal modes [33–36].

In order to explain at least qualitatively the behavior of LO modes in the NGIA IR spectra of charged crystalline Nb_2O_5 films, simple model calculations of LO spectra were made. Accordingly, we changed the refractive indices (*n*) by increasing numerically their values in the spectral range where the minimum refractive index (*n*) appears. Calculated LO spectra [$\mathrm{Im}(-1/\tilde{\varepsilon})$] showed the decrease in the intensity of the LO mode (Fig. 23). Neither an increase in the absorption coefficient (*k*) values of the polaron mode nor its decrease (not shown) gave rise to the experimentally found decrease in intensity of the LO mode. This clearly shows that experimentally determined decreases in the intensity of the LO mode in spectra of charged crystalline films are solely due to the optical effects stemming from the presence of the polaron mode, influencing the real part of the refractive index (*n*) in the vicinity of the LO mode. This suggests that changes in the LO mode with charging

Fig. 20 NGIA IR reflection/absorption spectra of **a** xerogel films and films obtained by heat treatment at **b** 300 °C and **c** 500 °C
Fig. 21 Ex situ NGIA IR spectra of Nb_2O_5 film heat treated at 300 °C
Fig. 22 Ex situ NGIA IR spectra of Nb_2O_5 film heat treated at 500 °C
Fig. 23a, b Model calculations of IR NGIA spectra (LO modes) of Nb_2O_5 films (TT-phase) at various states of cathodic charging. **a** *n1*: Calculated refractive index (*n*) spectrum from Kramers-Krönig analysis of near-normal (6 °) reflection spectra of pressed powders with TT-phase (Fig. 14a) *n1a-n1d*: numerically changed *n* values. **b** Calculated $\mathrm{Im}(-1/\tilde{\varepsilon})$ (LO modes) spectra with *n1-n1*d taken from Fig. 23a

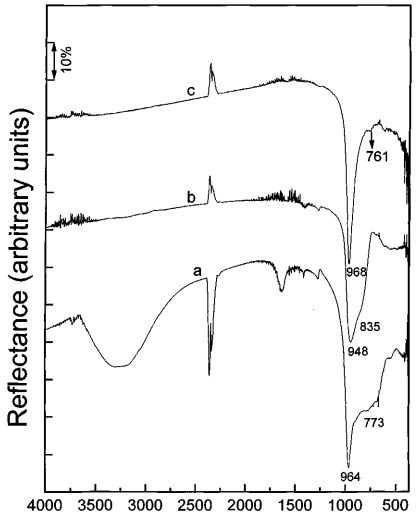

20

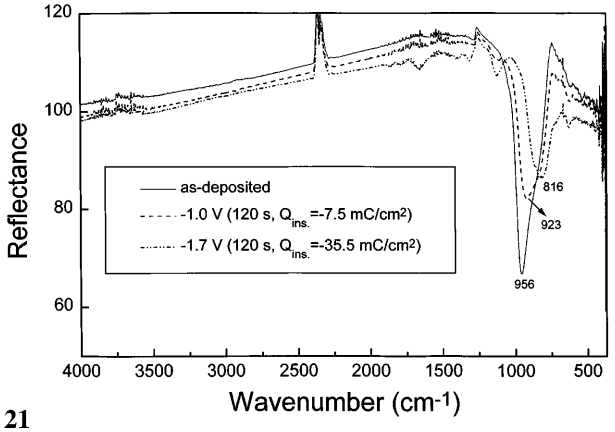

21

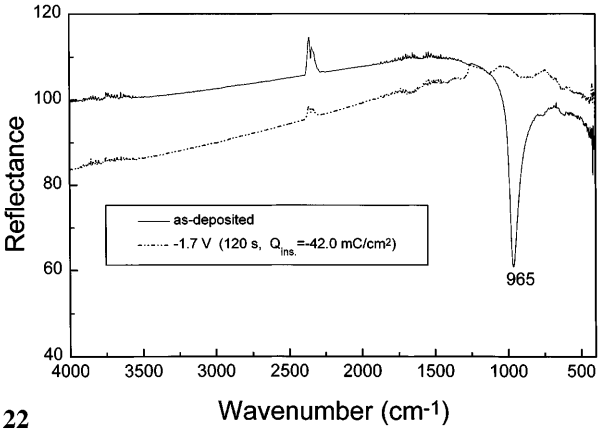

22

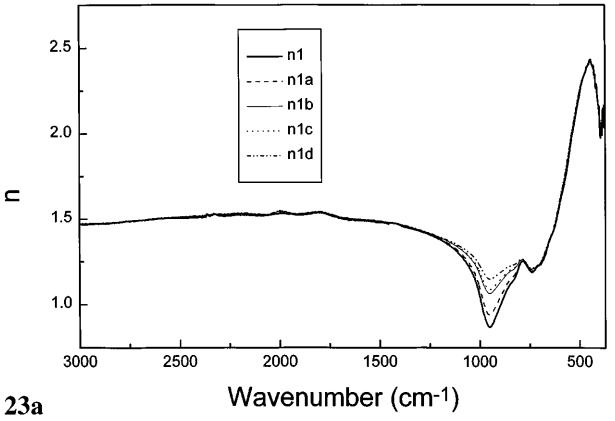

23a

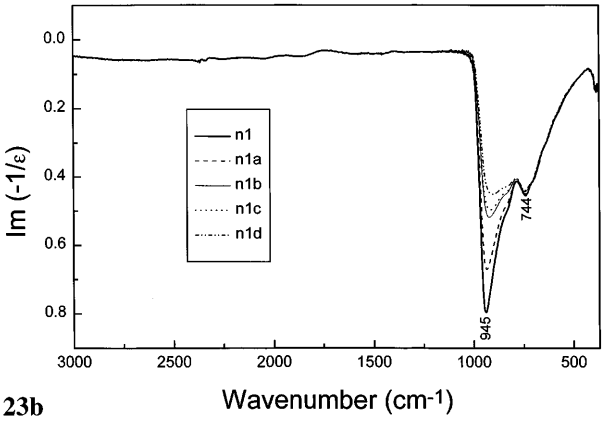

23b

could not be correlated with or interpreted in terms of intensity and frequency changes of the corresponding TO mode. This effect is greatest for strong polar modes that exhibit large TO-LO splitting with concurrent well-pronounced dispersion.

Discussion

Ex situ XRD spectra of charged films in the TT-phase and the reported XRD spectra of charged powders with the T-phase [11], together with presented ex situ IR

spectra of the TT-phase, gave sufficient information to establish that structural distortions of both types of film occur when Li^+ ions are inserted. This is important because it increases the ability of electrons to hop from one ion to another by absorbing the photons, giving rise to polaron absorption. The splitting of the Nb_3-O stretching mode clearly shows pronounced distortions in the structure of the TT- and T-phases with charging and corroborates the appearance of polaron absorption in IR spectral range of these two phases. Conversely, amorphous films do not exhibit polaron absorption in the IR spectral range, since only a relatively weak absorption was noted in the in situ UV-Vis spectra of charged films. This agrees with the weaker electrochromic changes detected for the latter phase.

The appearance of polaron absorption in the ex situ IR spectra suggests that the crystalline phase of Nb_2O_5 can be ranked among other electrochromic materials like amorphous WO_3 and crystalline V_2O_5 [1], where topochemical changes accompany the Li^+ ion insertion/extraction reactions. This is not surprising, since Nb_2O_5 is characterized by the high ionicity of the Nb-O bond. The strong ionic character of Nb_2O_5 crystalline and amorphous films is fully supported by the large LO-TO splitting established experimentally from the measured NGIA IR spectra; this is also confirmed from the calculated $\mathrm{Im}(-1/\tilde{\varepsilon})$ values obtained from the near-normal reflection spectra of pressed powders. Accordingly, from the well pronounced ionicity of Nb_2O_5, it is expected that when Li^+ ions are inserted into the structure a strong electrostatic repulsion is established between the inserted Li^+ ions and the cation framework. This results in a strong modification of the spatial charge distribution leading to distortions of the TT- and T-phases with Li^+ ion insertion. Ex situ XRD spectra of charged films showed that distortions are more pronounced for the TT-phase than for the T-phase, where Li^+ ion insertion do not lead to a change in the unit cell dimensions [11]; however, this was found for the TT-phase. Despite this, the cycling stability and electrochromic reversibility of the TT-phase is remarkably high, giving rise to reversible coloring/bleaching changes with cycling. Nevertheless, it is reasonable to expect that the cycling stability of the T-phase is higher than that of the TT-phase because diffraction analysis revealed no changes in the unit cell dimensions of the T-phase [11]. Atomic rearrangement does occur, with Li^+ ion insertion corroborating the splitting of the Nb_3-O stretching mode observed in ex situ IR spectra of charged films. Unfortunately, it is impossible to obtain further data about the electrochromic properties of Nb_2O_5 in the T-phase because the deposition temperature (800 °C) is too high to produce this type of film on conductive and optically transparent electrodes.

Amorphous films exhibit smaller electrochromic changes than do crystalline films. This is in accordance with the relatively small binding energy shifts of $Nb3d_{5/2}$, $Nb3d_{3/2}$ and O1s peaks in ESCA spectra which these films exhibit with Li^+ ion insertion [19, 20]. Ex situ IR spectra results support this because Li^+ ion insertion causes a change only in the intensity of the Nb-O stretching mode and not its frequency. At least six cycles are needed to attain reversible coloring/bleaching changes. After the precycling period, the coloring/bleaching changes are reversible, although the transmittance of the bleach state is always lower than that in the as-deposited films. This suggests that the structure of as-deposited films changes with cycling to produce a new electrochromically active phase characterized by Nb^{4+} redox sites retained in the discharged state. The changes in intensity noted in the ex situ IR spectra of charged films suggest that the structural modifications accompanying Li^+ ion insertion are small. Accordingly, the polaron absorption does not appear in the IR spectral range, confirming the weaker electrochromism of amorphous films.

The strong polaron absorption that appears in IR transmission spectra of charged crystalline films rules out the possible quasi-free electron reflection which characterizes the partially reduced H-Nb_2O_5 phase [50, 51]. The presence of quasi-free electrons helps to create the H-Nb_2O_5 phase's metal-like properties, which are manifested by the high reflection at wavelengths longer than the plasma wavelength (>1400 nm). IR spectra of our films do not exhibit such spectral properties, which agrees with the absence of ReO_3-type blocks in the structures of TT- and T-phases and are otherwise characteristic of the partially reduced H-Nb_2O_5 phase [9, 50, 51]. On the basis of these results the TT- and T-Nb_2O_5 films exhibit dominant polaron absorption, and the contribution from the quasi-free electrons is negligible.

Finally, NGIA IR spectra of charged/discharged films deserve some comments. Our previous ex situ IR spectroelectrochemical studies of various electrochromic films in colored and bleached states proved the usefulness of this type of measurement for the evaluation of the structural properties of films in charged/discharged states [17, 18, 33–38]. The main advantages of ex situ NGIA IR spectroscopic measurements are the absence of the usual highly absorbing electrolyte and the increased sensitivity of this method. An improvement in sensitivity of about 50 times that of the transmission measurements is common [32]. However, the main disadvantage of NGIA IR ex situ measurements is that the LO modes are shifted away from their TO counterpart modes observed in the absorption spectra of films, the LO-TO splitting depending on the ionicity of the film structure. This is not detrimental to carrying out vibrational mode analysis if the LO modes can be obtained independently by calculating the $\mathrm{Im}(-1/\tilde{\varepsilon})$ values with the help of a Kramers-Krönig analysis or can be determined experimentally using NGIA IR spectroscopy. The main problem, however, is the correct interpretation of the changes which the observed LO modes exhibit with charging, because the shifts in frequency of these modes are not related to changes in bond strength but are

rather dependent upon the change in intensity of the TO modes. IR spectroscopy of charged amorphous films clearly shows that the shift in frequency of the LO mode is related to the decrease in intensity of the TO mode.

The situation is more unclear for crystalline films, where the LO mode is extinct in the NGIA LO spectra of negatively charged films. This phenomenon appears to be general, and was recently noted for the amorphous electrochromic WO_3 films prepared via the peroxo-sol-gel route [17]. Two conditions must be met in order that the intensity of the LO mode drops to almost zero. First, the polaron mode must be present in the spectral range where the skeletal modes exist, and second, the LO-TO splitting must be high enough to cause a large dispersion of the skeletal modes. Simple model calculations showed that the decrease in intensity of the LO mode was caused by change of the refractive index (n) in the spectral range where the LO mode appears.

This result is important and suggests that the reported red shifts of the LO modes for various electrochromic films in different redox states must be reconsidered. However, for films with weakly expressed ionicity such as Ni hydroxide [33], the NGIA IR spectra could still be used for detecting the structural changes related to the redox processes in films and the presence of new phases. For these films where the polaron absorption extends into the frequency range of the skeletal modes, transmission spectra of charged films are needed to extract structural information about their redox states.

Conclusions

The sol-gel route has allowed us to make, via dip-coating deposition and heat treatment, Nb_2O_5 films exhibiting amorphous (ambient temperature, 300 °C) and crystalline structures corresponding to the pseudohexagonal TT- (300–550 °C) and orthorhombic T-phases (800 °C). IR and Raman spectra of powders are typical for certain phases. The observed differences between the spectra of deposited films in various crystalline modifications allowed assign us to the most prominent Nb-O bands, distinguishing the Nb-O streching modes of the xerogel and amorphous (300 °C) films ($\sim$560–600 cm^{-1}) and the Nb_3-O stretching characteristic of the crystalline phases from the Nb_3-O vibrating structural units. Nb_3-O stretching appearing in the TT-phase exhibited pronounced splitting, indicating strong distortion of the pseudohexagonal unit cell when Li^+ ions are inserted. This brings about electron hopping between the different sites in the films and gives rise to the strong polaron mode and strong electrochromic effect. In the T-phase the Nb_3-O stretching appears as a doublet, which is in accordance with its orthorhombic symmetry. The polaron absorption, similar to the TT-phase, became apparent in the spectra of charged films with the T-phase. However, the observed changes in the Nb_3-O stretching mode in charged spectra are not as pronounced as they are in spectra of the TT-phase. Conversely, ex situ IR spectra of the redox states of amorphous (300 °C) films showed variations in intensity of the Nb-O stretching mode (577 cm^{-1}), explaining the red shift of the LO mode, with charging detected in the NGIA IR spectra of charged films.

The reversibility of the redox processes in charged/discharged films observed using IR spectroscopy confirmed the results obtained from the in situ UV-Vis spectroelectrochemical measurements. All the films exhibited reversible electrochromic changes, which are much higher for films with the TT-phase than for amorphous (300 °C) films.

NGIA IR spectra of charged/discharged films differ considerably with respect to transmission spectra. This was explained by the large LO-TO splitting, which was corroborated from the calculated LO spectra $[\mathrm{Im}(-1/\tilde{\varepsilon})]$ obtained from the near-normal reflection spectra of powders. The decrease in the intensity of the LO band in the spectra of charged films was explained by using model calculations. Variations of the refractive index values were found to influence the behavior of the LO mode, decreasing its intensity in the spectra of charged films where polaron absorption appeared.

IR spectroscopic and XRD results revealed that despite the anisotropic unit cell dimension changes noted for the TT-phase with Li^+ ion insertion, the corresponding structural changes do not bring about irreversibility of the observed coloring/bleaching changes of the TT-phase. This contrasts with the relatively poor cycling stability of layered electrochromics such as $LiNiO_2$ [52] where development of new redox phases leads to deterioration of their electrochromic and electrochemical stability. This substantiates further studies of Nb_2O_5 films for electrochromic and battery applications.

Acknowledgements The authors wish to thank to Ministry for Science and Technology of Slovenia for financial support. This work was done within the framework of the Joule III "SmartWin" project (Pilkington, UK). M.M. also thanks the Ministry for her PhD Scholarship.

References

1. Granqvist CG (1995) Handbook of inorganic electrochromic materials. Elsevier, Amsterdam
2. Schäfer H, Gruehn R, Schulte F (1966) Angew Chem 78: 28
3. Kato K (1976) Acta Cryst B32: 764
4. Wells AF (1962) Structural inorganic chemistry. Clarendon Press, Oxford
5. Gatehouse BM, Wadsley AD (1964) Acta Cryst 17: 1545
6. Kato K, Tamura S (1975) Acta Cryst B31: 673
7. Holser WT (1956) Acta Cryst 9: 196
8. Schäfer H, Schulte F, Gruehn R (1964) Angew Chem 76: 536; (1964) Angew Chem Int Ed Engl 3: 511
9. Ikeya T, Senna M (1988) J Non-Cryst Solids 105: 243
10. Cho NH, Kang HB, Kim YH (1994) Ferroelectrics 152: 43
11. Kumagai N, Tanno K, Nakajima T, Watanabe N (1983) Electrochim Acta 28: 17
12. Kumagai N, Tateshita Y, Takatsuka Y, Baba M, Ikeda T, Tanno K (1995) J Power Sources 54: 175

13. Avellaneda CO, Macêdo MA, Florentino AO, Barros Filho DA, Aegerter MA (1994) SPIE 2255: 422
14. Avellaneda CO, Macêdo MA, Florentino AO, Aegerter MA (1994) SPIE 2255: 38
15. Aegerter MA, Avellaneda CO, Pawlicka A, Atik M (1997) J Sol-Gel Sci Technol 8: 689
16. Granquist CG (1995) Handbook of inorganic electrochromic materials. Elsevier, Amsterdam, Chaps. 2–11
17. Maček M, Orel B, Opara Krašovec U (1997) J Electrochem Soc 144: 3002
18. Maček M, Orel B, Sol Energy Mater Sol Cells (in press)
19. Özer N, Barreto T, Büyüklimanli T, Lampert CM (1995) Sol Energy Mat Sol Cells 36: 433
20. Özer N, Rubin MD, Lampert CM (1996) Sol Energy Mat Sol Cells 40: 285
21. Jehng JM, Turek AM, Wachs IE (1992) Appl Catal A 83: 179
22. Reichman B, Bard AJ (1981) J Electrochem Soc 128: 344
23. Gomes MAB, Bulhões LOS, Castro SC, Damiao AJ (1990) J Electrochem Soc 137: 3067
24. Dyer CK, Leach JSL (1978) J Electrochem Soc 125: 23
25. Aleshina LA, Malinenko VP, Phouphanov AD, Jakovljeva NM (1986) J Non-cryst Solids 87: 350
26. Yoshimura K, Miki T, Iwawa S, Tanemura S (1995) Jpn J Appl Phys 34: L1293
27. Machida N, Tatsumisago M, Minami T (1986) J Electrochem Soc 133: 1963
28. Yao JN, Loo BH, Hashimoto K, Fujishima A, Ber Bunsenges (1992) Phys Chem 96: 699
29. Lee RG, Crayston JA (1991) J Mater Chem 1: 381
30. Ohtani B, Iwai K, Nishimoto S, Inui T (1994) J Electrochem Soc 141: 2439
31. Faria RC, Bulhões LOS (1994) J Electrochem Soc 141: L29
32. Suëtaka W, Yates JT (1995) Surface infrared and Raman spectroscopy. Plenum Press, New York
33. Šurca A, Orel B, Pihlar B, Bukovec P (1996) J Electroanal Chem 408: 83
34. Šurca A, Orel B, Cerc-Korošec R, Bukovec P, Pihlar B (1997) J Electroanal Chem 433: 57
35. Švegl F, Orel B, Hutchins MG, Kalcher K (1996) J Electrochem Soc 143: 1532
36. Švegl F, Orel B, Bukovec P, Kalcher K, Hutchins MG (1996) J Electroanal Chem 418: 53
37. Orel B, Maček M, Švegl F, Kalcher K (1994) Thin Solid Films 246: 131
38. Orel B, Lavrenčič Šangar U, Hutchins MG, Kalcher K (1994) J Non-cryst Solids 175: 251
39. Lavrenčič Štangar U, Orel B, Régis A, Colomban PH, J Sol-gel Sci Technol 8 (1997) 965
40. McConnell AA, Anderson JS, Rao CNR (1976) Spectrochim Acta 32A: 1067
41. Jehng JM, Wachs IE (1991) Chem Mater 3: 100
42. Grosse P (1990) Vib Spectrosc 1: 187
43. Farmer VC (1974) The infrared spectra of minerals. Mineraological Society, London, pp 183–205
44. X-ray powder diffraction file JCPDS-ICDD (1993) Newtown, Pa
45. Isidorsson I (1996) PhD thesis. Uppsala
46. Opara Krašovec U, Orel B, Hočevar S, Muševič I (1997) J Electrochem Soc 144: 3398
47. Bhide V, Husson E, Gasperin M (1980) Mater Res Bull 15: 1339
48. Husson E, Repelin Y, Dao NQ, Brusset H (1977) Mater Res Bull 12: 1199
49. Nakamoto K (1986) Infrared and Raman spectra of inorganic and coordination compounds, 4th edn. Wiley, New York
50. Rüscher C, Salje E, Hussain A (1988) J Phys C: Solid State Phys 21: 3737
51. Rüscher CH (1992) Physica C 200: 129
52. Dahn JR, Sacken U, Michal CA (1990) Solid State Ionics 44: 87